



Full paper

Energy from greenhouse plastic films[☆]Hao Wang^a, Maoyuan Zhang^{a,b}, Ze Yang^{a,c}, Zhaozheng Wang^{a,d}, Xu Liu^a, Yijia Lu^a,
Linhong Ji^{a,*}, Zhong Lin Wang^{d,e,**}, Jia Cheng^{a,*}^a State Key Laboratory of Tribology, Department of Mechanical Engineering, Tsinghua University, Beijing 100084, China^b School of Electromechanical and Automotive Engineering, YanTai University, Shandong 264005, China^c School of Engineering and Technology, China University of Geosciences (Beijing), Beijing 100083, China^d Beijing Institute of Nanoenergy and Nanosystems, Chinese Academy of Sciences, Beijing 101400, China^e School of Materials Science and Engineering, Georgia Institute of Technology, Atlanta, GA 30332-0245, USA

ARTICLE INFO

Keywords:

Greenhouse Energy

Greenhouse

Triboelectric Nanogenerator

Intelligent agriculture

ABSTRACT

Greenhouses are occupying worldwide vast cultivated land for plantation. The polymer film covered on most greenhouses is exactly a ready-made triboelectrification layer for Triboelectric Nanogenerator (TENG). However, so far, such a huge area of polymer film is still underutilized. Generally, the larger area of the triboelectric film, the better performance of TENG output. Therefore, a new concept of Greenhouse Energy is proposed, which refers to various effective energy directly or indirectly generated by means of greenhouse film. As a typical example of Greenhouse Energy, a model greenhouse based on TENG with transparent electrodes and triboelectric layers is demonstrated. The technologies of charge pumping and switch circuit are adopted to improve the output performance. As a demonstration, the commercial temperature and humidity sensors could be powered for about 20 s after capacitors charged for 500 s. The output power density reaches 3.06 mW/m². As a reasonable deduction, if a real greenhouse with tens of square meter is constructed in the same way, it will become a promising distributed power source for powering devices such as sensors, controllers, lights, irrigation system in intelligent agriculture. This work aims to pave the way for the application of TENG in the field of agriculture and to provide a new possibility for intelligent greenhouses. Starting from agricultural field, Greenhouse Energy will collaborate with Blue Energy further complementing the new distributed energy system.

1. Introduction

With the emergence of agriculture, human beings finally got rid of the long-term migration for gathering and hunting, and then was able to develop today's civilization in the form of settlement in a relatively stable environment. The development stage of agriculture is often reflected in people's utilization of environmental resources. As early as Roman times, there was a record of using sheets of selenite as a shelter to grow cucumbers for the emperor [1]. In 1800, the first practical modern glass greenhouse was proposed [2]. The light and heat of the sun began to be used more effectively, breaking through the seasonal limitations of agricultural production. In the 1950s, polyethylene (PE) ushered in rapid development and PE film began to be widely used [3,4]. The subsequent sharp drop in material cost made it possible to spread

greenhouses from aristocratic manors finally to ordinary farms. Until today, in conventional agricultural production, greenhouses, as mature agricultural facilities, have been used worldwide. Among them, most of the greenhouses, high polymer materials such as plastics are still the mainstream film materials. While fully demonstrating its application value and far-reaching impact, it is also thought-provoking whether such a huge and ready-made greenhouse film area in the whole world can bring us MORE besides simply insulation and moisturizing before it becomes "white pollution".

Nowadays, intelligent agriculture has become an emerging research hotspot in many countries. This includes the transformation from a traditional greenhouse with simple structure, single function and few supporting facilities to a new generation of greenhouse with standardization, intensification and intelligentization. The prime topic must be

[☆] "Prof Zhong Lin Wang, an author on this paper, is the Editor-in-Chief of Nano Energy, but he had no involvement in the peer review process used to assess this work submitted to Nano Energy. This paper was assessed and the corresponding peer review managed by Professor Chenguo Hu, an Associate Editor in Nano Energy."

* Corresponding authors.

** Corresponding author at: Beijing Institute of Nanoenergy and Nanosystems, Chinese Academy of Sciences, Beijing 101400, China.

E-mail addresses: jilh@tsinghua.edu.cn (L. Ji), zhong.wang@mse.gatech.edu (Z.L. Wang), chengjia@tsinghua.edu.cn (J. Cheng).

<https://doi.org/10.1016/j.nanoen.2021.106328>

Received 25 April 2021; Received in revised form 2 July 2021; Accepted 7 July 2021

Available online 15 July 2021

2211-2855/© 2021 Elsevier Ltd. All rights reserved.

faced in achieving the above-mentioned transformation is the energy. Undeniably, the emergence of photovoltaic devices has provided an attractive choice for the environmentally friendly and renewable electricity demand of greenhouses. A lot of research work has been carried out in this field [5–9]. But objectively, photovoltaic devices are greatly restricted by the weather, in other words, it is difficult to work ideally on rainy days. And most of photovoltaic materials themselves are opaque, making it difficult to directly bond with the greenhouse film. Even if some transparent photovoltaic materials have been proposed [10–14], there will be inevitable problems such as reduced energy harvest capacity, increased price and increased manufacturing difficulty.

On the other hand, although wind energy can be considered as another kind of developed renewable energy, there is still few mature way of utilization, including wind turbines, at this stage. However, it is difficult to integrate huge wind turbines directly with the greenhouse. If a large-scale wind farm is used as indirect power supply, it cannot be regarded as the greenhouse itself relying on wind energy to achieve self-powered. At the same time, there are always problems such as high price, serious land occupation [15], difficult manufacturing, difficult dispatching [16] and poor power-grid-friendliness [17,18]. Some small-scale wind turbines might be able to be installed around the greenhouse. They are undeniably a kind of alternative choice, but none of them have a commercial mass production yet. In other words, there is still no convenient and mature technology to directly harvest wind energy in agricultural greenhouses. Therefore, a new attempt from another perspective is considered.

Worldwide, today's greenhouse agriculture still has significant labor-intensive properties, and research on intelligent agriculture is just in its infancy. Limited by the above-mentioned deficiencies of the solar and wind energy technologies, the research on the combination of renewable energy and greenhouse-agriculture has not yet obtained a satisfactory solution. Only by finding a new technology that can better make use of the environment energy and give full play to the advantages of the greenhouse films, can it provide new possibilities for the realization of intensification and intelligentization in greenhouse-agriculture.

In 2012, Zhong Lin Wang's team proposed the world's first TENG [19], bringing a brand-new choice to the world's energy and sensor technology. There have been numerous applications of TENG in medical [20,21], biological [22,23], sensing [24–27], wave energy [28,29], plasma [30,31] and other fields [32–37], while there are still few explorations in the field of agriculture. Excellent insulating materials, including various plastics, are exactly the triboelectric materials commonly used by TENG. These materials tend to have low cost, low difficulty in obtaining, high transparency, good flexibility and stable physicochemical properties [38–41], which directly make them have sufficient innate advantages in combination with greenhouses. Furthermore, a major factor limiting the output performance of TENG lies in its "2D power generation" feature. That is, different from the "3D power generation" of conventional electromagnetic generator (EMG), TENG has to rely on sufficient contact area to achieve adequate charge transfer. That is, the larger area of the triboelectric film, the better performance of TENG output. Previously, most TENGs were small devices (mostly several to tens of square centimeters), so their power generation was severely limited. As mentioned above, greenhouses can provide extremely large and ready-made film area, which just becomes the biggest advantage for the combination of TENG and greenhouses. In addition, in greenhouses' environment, low-frequency energy such as wind energy is abundant. TENG precisely has a higher efficiency for harvesting such low-frequency (<5 Hz) mechanical energy, compared with EMG [42–44].

Based on the above conditions, a new type greenhouse based on TENG was designed. The contact-separation mode TENG, which is composed of greenhouse films, can harvest environmental mechanical energy (mainly wind energy) and convert it into electrical energy to supply the greenhouse system.

1.1. Greenhouse Energy

With abovementioned new-designed greenhouse as a prompt, a corresponding concept, Greenhouse Energy, is proposed here, as shown in Fig. 1. Greenhouse Energy refers to all the energy directly or indirectly generated by the covering films of the greenhouse. For example, it includes not only the conventional thermal energy collected by the plastic film, but also the electric energy generated by the new TENG-greenhouse. The obtained energy will be fed back to the operation and production of greenhouses again. And eventually a self-powered closed-loop system including greenhouses as the key part will be formed to serve the establishment and practice of intelligent agriculture. Greenhouse Energy will collaborate with Blue Energy (the concept for ocean wave energy) [45], further complementing the new distributed energy system starting from agricultural field.

2. Results and discussion

2.1. Design and electric characteristics of CST-greenhouse

In order to facilitate the experiment to verify the function, a small-scale test model (Contact & Separation TENG Greenhouse, CST-Greenhouse) was designed and fabricated, as shown in Fig. 2a₁. Two common and low-cost plastics, polyethylene terephthalate (PET) and Polyethylene (PE), were chosen as triboelectric materials, which have sufficient electrical differences in the triboelectric series [46]. Indium tin oxide (ITO), which has both conductivity and transparency, was selected as the electrode coated over the PET film. CST-Greenhouse adopts the contact-separation mode TENG, in which the mutual movement between the movable frame and the fixed frame are utilized to generate charge transfer. The states of contact and separation are shown in Fig. 2b. Charge pump technology is a widely recognized technology to enhance the output capacity of TENG, so it has also been integrated into the design of this CST-Greenhouse. The principle and promotion of the charge pump will be described in detail later in Section 2.2. While in this section, the overall structure and performance of the greenhouse will be discussed first. The main greenhouse (the left part in Fig. 2a₁, namely Main TENG) has a certain difference from the smaller one as charge pump (the right part in Fig. 2a₁, namely Pump TENG). That is, Pump TENG is an ordinary TENG with only two electrode layers, but the Main TENG needs to have three electrode layers to form an approximate variable capacitor and a constant capacitor in series, so as to achieve the abovementioned enhancement effect. The material distribution of each film layer is already shown in Fig. 1. It should be noted that actually there is no need for such a gap between Main TENG and Pump TENG. These two TENGs could be in the same frame with appropriate insulation, as shown in Fig. S1. When it comes to a real-scale CST-Greenhouse rather than this small one, the multilayer films could be divided into an appropriate number of segments in length direction. Also, the area ratio and the distribution of Main and Pump TENG could be adjusted and optimized according to the actual situation. These segmented movable frames can be set to synchronize, or can be independent, as shown in Fig. S2. The charge transfer process during the movement cycle is shown in Fig. 2c. In more detail, the 1/4 arch keels on both sides of the fixed frame are combined at an angle of 0° to form an approximate standard semicircle. Instead, the 1/4 arch keels on both sides of the movable frame are combined at an angle of 12° (the angle of 12° can be adjusted according to the actual demand), so as to provide a maximum movement stroke of about 25 mm between the two frames. The detailed theoretical analysis of the relationship between angle and stroke is shown in Supplementary Note 1. At the extreme position, the two 1/4 arch keels on one side will be in full contact. It should be noted that the reason for adopting such a symmetrical oscillating structure is that it can always maintain the synchronous contact and separation of the huge films, thereby optimizing the output performance. If simultaneous contact or separation of the films cannot be achieved, the changes



Fig. 1. Greenhouse Energy schematic. Energy generated by multilayer polymer films powers the operation of greenhouse system. Example materials of the multilayer films are given as PET, PE and ITO. Sensors, including temperature, humidity, photoelectric and CO₂ sensors, will monitor the real-time condition of the greenhouse. All information will be transmitted to the control terminal to arrange the operation of different equipment, e.g. the opening degree of the vent, the intensity of the supplementary lighting, the switch of the irrigation system. The greenhouse itself will become a self-powered closed-loop feedback system. Greenhouse Energy will contribute to the establishment of a further complete distributed energy system.

in the electric field will cancel each other to a certain extent, then the transfer-charge amount will be reduced, resulting in a decreased output. The movement of the model is shown in Supplementary Video S1.

Supplementary material related to this article can be found online at [doi:10.1016/j.nanoen.2021.106328](https://doi.org/10.1016/j.nanoen.2021.106328).

Under different intensities of external force, the movable frame will show different motion states, which need to be evaluated separately. In the experiment, a linear motor was used to push the movable frame, simulating greenhouse's motion state under external disturbances. With the help of this linear motor, more standardized and reproducible data could be obtained. First, the rectified open circuit voltage (V_{oc}) and short circuit current (I_{sc}) values are measured. The experimental circuit is shown as Fig. 2a₂. According to experiments, under a fixed frequency of 2 Hz, with the increase of movement amplitude (the maximum stroke: 25 mm), both the open circuit voltage and short circuit current increase significantly, as shown in Fig. 2d and e. This is consistent with the expected results based on mechanism analysis. That is, the greater the amplitude, the greater the change in greenhouse's capacitance, then the greater the amount of charge transferred. The corresponding relationship between amplitude and capacitance is shown in Fig. S3a. The relationship between amplitude and external force is shown in Fig. S3b. When moving at the maximum amplitude, V_{oc} exceeds 160 V and the peak value of I_{sc} exceeds 1 μ A. On the other hand, under a fixed amplitude of 25 mm, with the increase of the vibrate frequency (the maximum test frequency: 5 Hz), I_{sc} increase significantly, while V_{oc} increase slightly, as shown in Fig. 2f and g. Theoretically, the vibration frequency changes directly affect the amount of charge transfer per unit time, and therefore the current change is significant. On the contrary, assuming that in an ideal condition, when the moving amplitude remains the same, the total amount of charge transfer is the same, so that the generated electric field is also the same. However, since the charge loss cannot be ignored in the actual experiment, the high-frequency contact is more conducive to keeping the charge on the film at a higher level. Therefore, the voltage rises slightly with increasing frequency. When the frequency is 5 Hz, I_{sc} exceeds 3.5 μ A and V_{oc} quickly exceeds the highest range of the electrometer (250 V). Therefore, the steady-state open circuit voltage cannot be accurately measured, and only a rising curve for 5 Hz is shown in Fig. 2 g.

It can be seen that under different external disturbances, CST-Greenhouse can effectively harvest mechanical energy and convert it into electrical energy. The photograph of the CST-Greenhouse

experimental model is shown in Fig. S4. Based on the above results, since the amplitude of 25 mm is a complete stroke, and the frequency of 2 Hz is relatively moderate and closer to the natural disturbance frequency, they are selected as the standard motion conditions to complete the subsequent experiments. Moreover, in order to further verify and demonstrate the feasibility and effectiveness of the CST-Greenhouse, some supplementary experiments under an artificial wind environment are shown in Supplementary Note 2.

2.2. Charge pump performance

As mentioned above, the design of a charge pump is introduced in CST-Greenhouse. The charge pumping mechanism is based on a floating conductive layer and injected bound charges from a charge pump, which can decouple the charge density and the intensity of friction [47]. It has been proven by many researches that charge pump has a quite good output enhancement effect [47–50]. The circuit and principle can be visually demonstrated by Fig. 3b. Generally, Pump TENG is an ordinary contact separated TENG with two electrode layers, while Main TENG has an additional electrode. The top electrode and the middle electrode of Main TENG form a "variable capacitor", and the middle electrode and the bottom electrode form a "constant capacitor". Pump TENG provides charge for the variable capacitor. The top electrode and the bottom electrode are connected to the output terminal. Theoretically, after Pump TENG charges the variable capacitor to saturation, the charge density on the top electrode and the middle electrode will remain constant. The change of the distance between the two plates of the variable capacitor will cause the flow of charge between the top plate and the bottom plate. A short section greenhouse with a smaller film area is used as a charge pump to provide charge to the main greenhouse, thereby achieving the desired effect.

In order to show the experimental model more intuitively, Pump TENG and Main TENG were built separately, as shown in Fig. 3a. However, in practical applications, there is no need for spatial separation, that is, Main TENG and Pump TENG are a unified whole. We only need to set an appropriate area as a charge pump and add reasonable circuits. In order to match the most common working environment of the greenhouse, the films have not been pre-polarized. Pre-polarization is a process of artificially adding charge to the material surface, which can greatly increase the surface charge density by corona discharge [51–53], so as to achieve the purpose of temporarily improving the

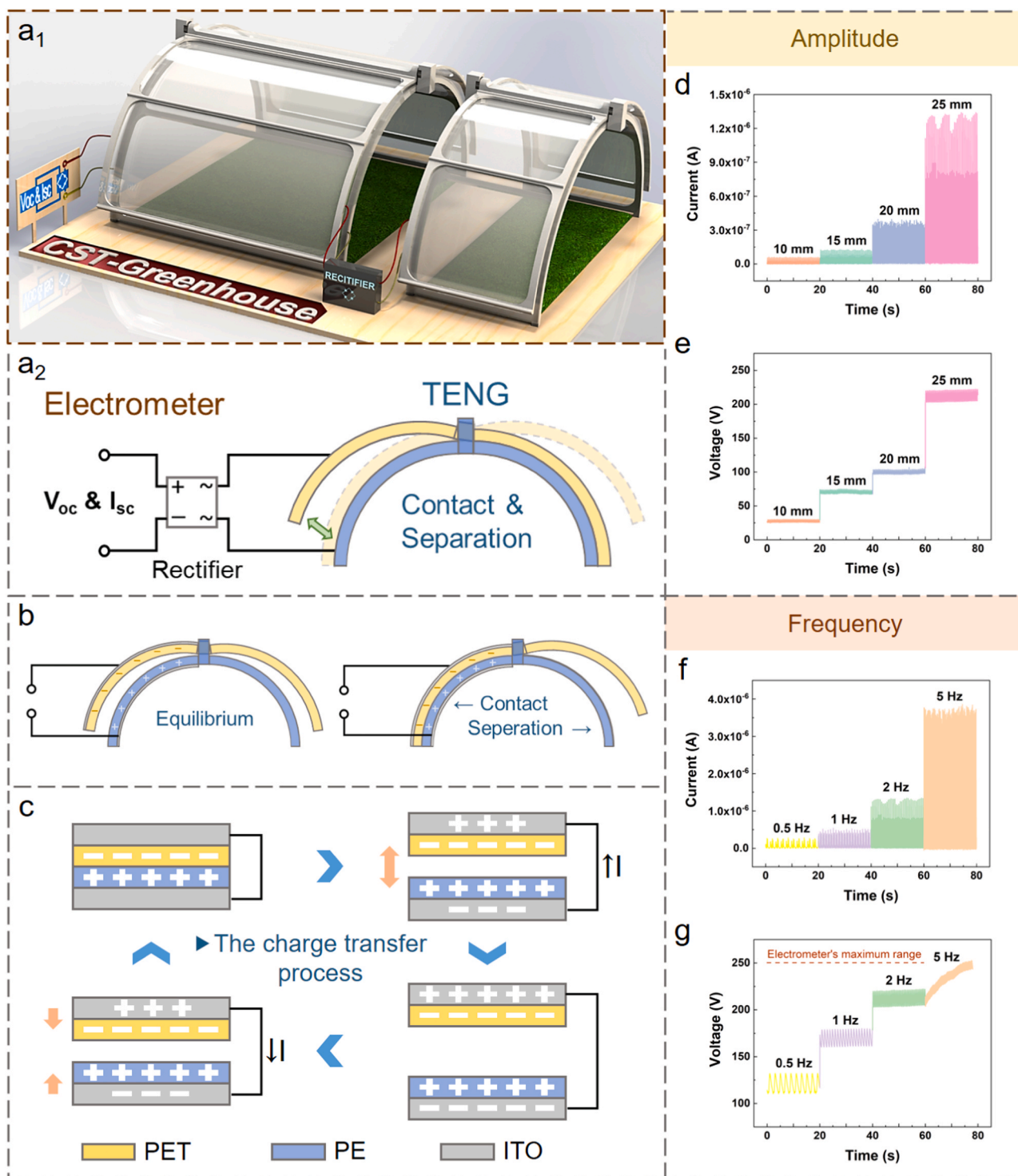


Fig. 2. (a₁) Structure diagram of CST-Greenhouse. (a₂) Schematic diagram of CST-Greenhouse. (b) The movement states of equilibrium, contact and separation of CST-Greenhouse. (c) The charge transfer status of TENG multilayer films. (d) (e) The short-circuit current and open-circuit voltage of the CST-Greenhouse with different movement amplitudes. (f) (g) The short-circuit current and open-circuit voltage of the CST-Greenhouse with different frequencies.

output-enhancing capability of charge pump. Although this will lead to the weakening of the pump effect, if it can still achieve the expected function, it will even show its practicality.

To demonstrate the effect of the charge pump, the output with and without charge pump was measured separately. First, the frequency characteristics of V_{oc} and I_{sc} are measured. The experimental results show that as the frequency increases, the enhancing effect of the charge pump becomes increasing obvious, as shown in Fig. 3c and d. When the

frequency is 2 Hz, it has about 3 times enhancing effect on both V_{oc} and I_{sc} . Consistent with the aforementioned, a frequency of 2 Hz is selected as the standard value, under which the performance of the greenhouse with different loads is determined.

Under different load resistances, the peak values and effective values of the output are respectively demonstrated, as shown in Fig. 3e~j. The experimental results show that the peak values and effective values of voltage and current are significantly improved under each load. In a

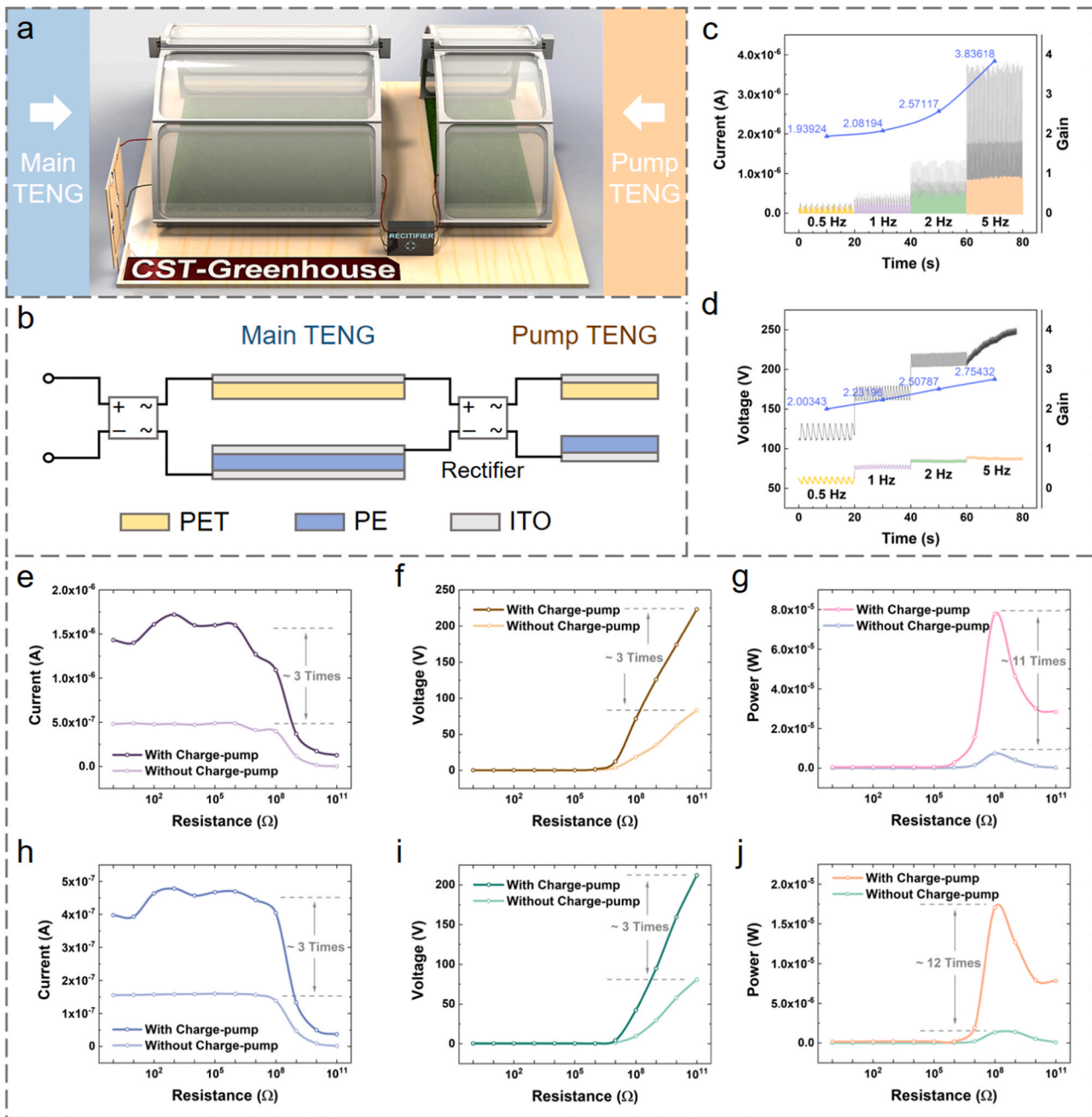


Fig. 3. (a) Model diagram of Main TENG and Pump TENG. (b) Schematic diagram of charge pump mechanism. Comparison of short-circuit current (c) and open-circuit voltage (d) with and without charge pump under different frequencies. The Colored curves are output without Pump TENG, while the gray curves are with Pump TENG. (e-j) The output comparison with and without charge pump under different load resistance. Peak output: (e) the peak load current, (f) the peak load voltage and (g) the peak load power. Effective output: (h) the effective load current, (i) the effective load voltage and (j) the effective load power.

larger range, the voltage and current have an approximate 3 times increase. When the external resistance is around $10^8 \Omega$, the output power reaches the maximum. In this state, the enhancing effect is more than 10 times. Here, it should be noted that in this small-scale experimental model, the area ratio of the Main TENG (S_{main}) to the Pump TENG (S_{pump}) is 2:1. That is, the area of the Pump TENG is not small enough to be ignored, so for the sake of rigor, the change in the overall film area should be taken into consideration. After adding an area coefficient, the power improvement effect per unit area is more than $\left(\text{Gain Per Area} = \text{Gain} \times \frac{S_{\text{main}}}{S_{\text{main}} + S_{\text{pump}}} = 10 \times \frac{2}{2+1} = 6.7 \right)$ times. Of course, in a real-scale CST-Greenhouse, the proportion of the area occupied by the charge pump is

very small, in other words, S_{pump} is a small quantity. Therefore, $\text{Gain Per Area} \approx \text{Gain}$. It can be seen that the addition of the charge pump has significantly improved the output capacity of CST-Greenhouse, which provides strong support for the practicality of the real-scale greenhouse.

2.3. Load performance

After verifying the effectiveness of the charge pump, the output characteristics of CST-Greenhouse under different external conditions need to be further measured and presented. The circuit diagram for measurement is shown as Fig. 4a. The waveform characteristics of voltage and current under loads are shown in Fig. 4b. The corresponding peak values of the output are shown in Fig. 4c-e. The effective values

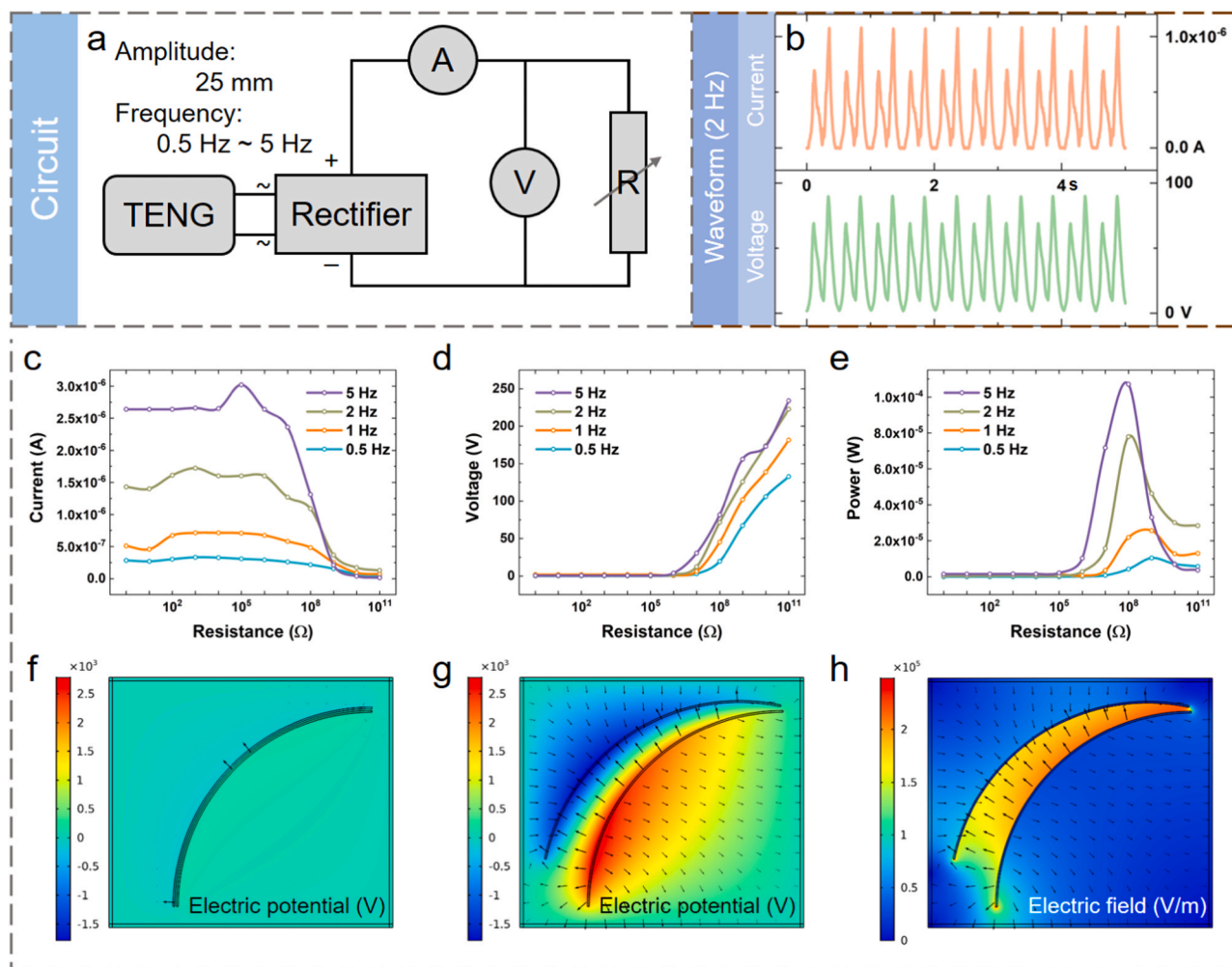


Fig. 4. (a) Experimental circuit diagram for measuring the performance under load. (b) The waveform of load current and load voltage. (c-e) The peak output of CST-Greenhouse with different load resistance and frequencies: (c) the peak load current, (d) the peak load voltage and (e) the peak load power. (f) The simulation electric potential distribution in contact state. (g) The simulation electric potential distribution in separation state. (h) The simulation electric field distribution in separation state.

are shown in Fig. S5. With the increase of frequency, the current and the power are obviously increased, while the voltage increases relatively slightly. Each parameter shows its corresponding uniform changing law. All these are consistent with the experimental results and mechanism analysis in Section 2.1. Similarly, it should be noted that when the frequency is 5 Hz and the load resistance is large, the voltage quickly approaches the maximum range of the electrometer, causing a certain deviation in the last two sets of values in Fig. 4d. If a high-voltage probe is added, although the measurement of the final stable value can be completed, the deviation will be even greater due to the charge loss brought in by probe itself (because the inner resistance of probe ≈ 1 G Ω). In addition, as the frequency increases, the peak of the power gradually shifts to the direction of small resistance, that is, the external load resistance corresponding to the maximum power gradually decreases. The theoretical basis is that the average impedance of TENG can be approximated as $1/f C_{\text{avg}}$, where f is the signal frequency of the voltage and C_{avg} is its average inherent capacitance [54]. Therefore, it can be seen that the increase of the vibration frequency f will lead to the decrease of the optimal resistance load.

In order to further demonstrate the operation process of CST-Greenhouse, COMSOL simulation is introduced to show its electrical status. The experiment with a frequency of 2 Hz was selected as the representative case for simulation. The load resistance with the highest power output (100 M Ω) is selected for the calculation of charge density.

According to the experimental data, the charge transferred Q in 10 s is about 2.927×10^{-6} C. The average charge density σ on each triboelectric film is about 2.043×10^{-6} C/m 2 . With above experimental data, the electric potential distribution in contact and separation states are shown in Fig. 4f and g. The electric field distribution in separation state is shown in Fig. 4h. It should be noted that the simulation results of maximum electric potential and electric field strength are reasonably much larger than the real condition, because the experimental conditions are far from perfect ideal. The specific setup in the COMSOL model is shown in Supplementary Note 3.

On the other hand, when the external load is capacitors, TENG can also effectively charge them. The picture of the experimental device is shown in Figs. 5a and S6. The capacitors can be thought of as a "battery" for charge storage. Therefore, what is expected is to charge the "battery" more efficiently and discharge it more stably. Therefore, the combination form of capacitors in this "battery" is essential. To this end, a switch circuit is added to the output, as shown in Fig. 5b. By triggering the switch, the conversion of the capacitors from charging in serial to discharge in parallel can be realized. Thereby, a larger current can be provided to meet the working requirements of commercial electronics. Furthermore, setting different numbers of capacitors (47 μ F) in the switch circuit will directly affect the charging time, discharging stability and working conditions of electrical appliances. The capability of CST-Greenhouse to charge and discharge the capacitors is shown in Fig. 5c.

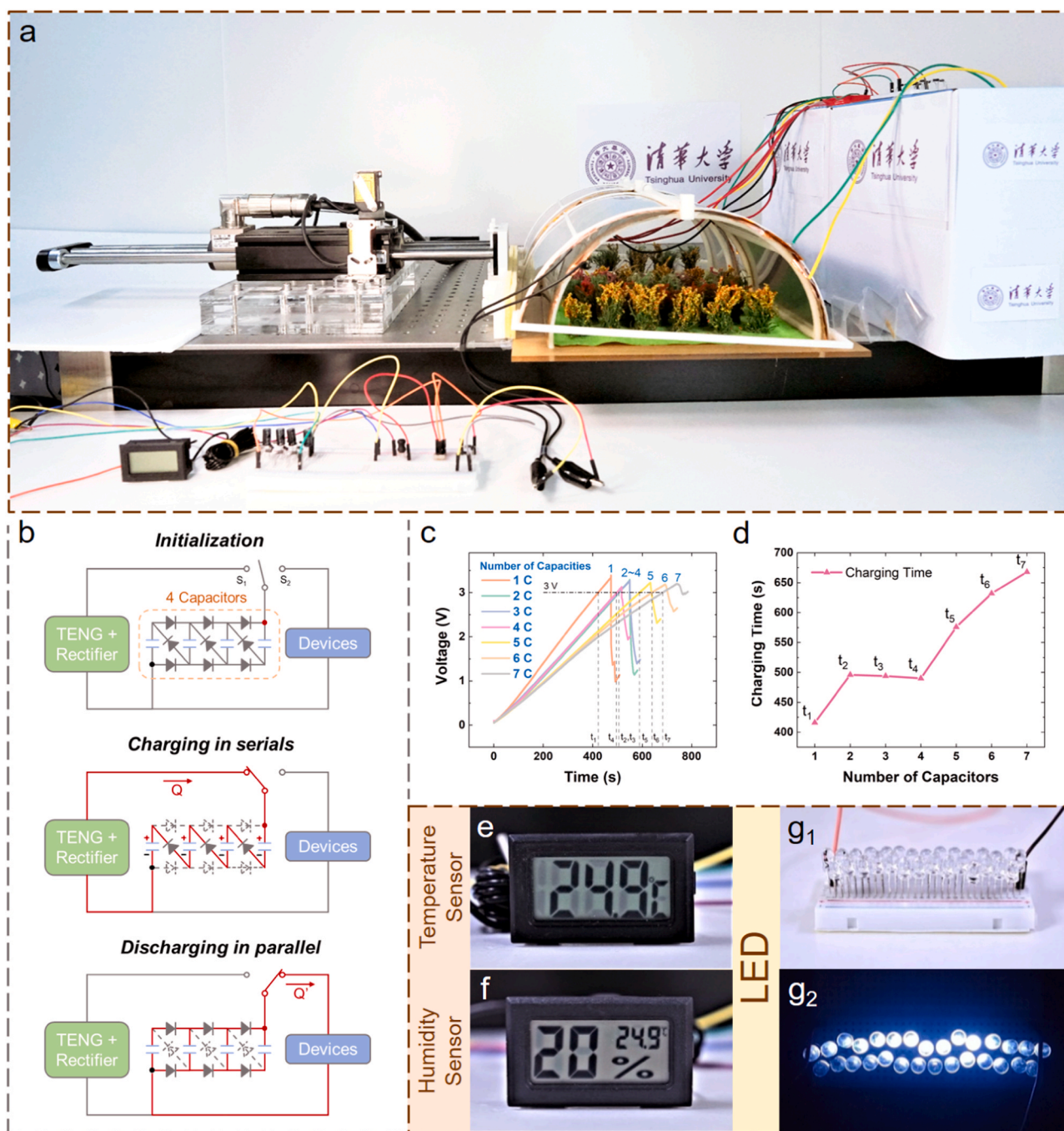


Fig. 5. (a) Photograph of CST-Greenhouse powering commercial devices. (b) Schematic diagram of the switching circuit. Switch between charging in serials and discharging in parallel. (c) The charging and discharging curves with different number of capacitors. (d) The charging time from 0 V to 3 V with different number of capacitors. (e) CST-Greenhouse powered temperature sensor. (f) CST-Greenhouse powered humidity sensor. (g) CST-Greenhouse powered LED.

The time to charge 1–7 capacitors from 0 V to 3 V is represented as t_1 to t_7 respectively. It can be seen that as the number of capacitors increases, the charging time presents 3 different stages, as shown in Fig. 5d. (1) Among them, when there is only one capacitor, it is only an ordinary capacitor working process. (2) When the number of capacitors is 2, 3 and 4, the charging speed is not much different. (3) When the number of capacitors is 5 or greater, the charge time starts to increase significantly. It should be noted that abovementioned “stage 2” in Fig. 5d is not an experimental error caused by, for example, failure of some capacitors. Because obvious difference can be seen at the discharge range (at the end of the curve in Fig. 5c), which proves that every capacitor is working. That is, they conform to the law that the more capacitors, the

higher the voltage level after discharge. The reason for this increasing voltage level is that the larger the total number of capacitors, the less charge each capacitor needs to transfer to supply the electrical appliances’ working, resulting in a smaller voltage drop after discharging. Therefore, it is necessary to further discuss the changing stages of charging time.

Combining the above phenomenon, the reasons for these three stages can be speculated. When charging, the capacitors are in serials and no inductance is added. It is definitely that more capacitors means a smaller equivalent capacitance C . Based on the impedance formula $Z = R + j(\omega L - 1/\omega C)$ with $\omega L \approx 0$, a larger $1/\omega C$ will result in greater load impedance. Therefore, it is reasonable to speculate from the experi-

mental results that when the number of capacitors is small (less than or equal to 4), the increase of the load impedance will lead the load and the greenhouse TENG to have a relative higher impedance matching degree, resulting in an improvement in the power generation capacity of CST-Greenhouse. For this reason, the slowdown in charging speed caused by the increase in capacitor number is not obvious. However, when the number further increases, the load impedance also further increases, leading to a decrease in the matching degree between the greenhouse and the external impedance. Therefore, the power generation capacity does not increase but decreases. In addition, coupled with increasing number of capacitors to be charged, the charging time is significantly increased. It should be noted that when the number of capacitors is 1, although the discharge is still completed, insufficient power will often cause the commercial devices to fail to work normally. In summary, the switch circuit composed of 4 capacitors can provide sufficient energy for the electrical appliances, while the charging time will not be too long. Therefore, 4 capacitors were selected to complete the subsequent application experiments.

2.4. Applications

The previous sections have fully demonstrated the feasibility of CST-Greenhouse from experimental data. In order to visually demonstrate the practical significance of CST-Greenhouse, some demonstrations are provided. Although the scale of the experimental model is really small, which means small triboelectric area and limited movement amplitude, if some application demonstrations can still be completed, the feasibility of the Greenhouse Energy scheme can be supplemented from the application point of view. The picture of the experimental device is shown in Fig. 5a and S4. The experimental circuits are shown in Fig. S7. When the greenhouse outputs directly without capacitors, about 30 LED lights can be lit, as shown in Fig. 5g.

When a switch circuit with 4 capacitors is used, CST-Greenhouse can successfully drive the normal working of commercial electrical appliances. For example, after charging for about 500 s, a digital temperature sensor or a humidity sensor can be powered for about 20 s, as shown in Fig. 5e and f. The internal resistance of the digital temperature sensor used is 242 Ω , and the internal resistance of the digital humidity sensor is 298 Ω . Refer to Fig. 4e, it can be known that such a small load is not in the satisfactory load range of output performance, so capacitors with switch circuit have to be added to complete the transformation of electrical energy. The rated voltage of the sensors is 1.5 V, the maximum working current is 4 μA , and the maximum working power is 6 μW . Since the stable current provided by the capacitors is not as large as commercial button battery, the capacitors need to be charged to 3 V to supply enough charge for sensor's working. The above experiment is sufficient to verify the feasibility of CST-Greenhouse supplying sensors for intermittent operation. It is not difficult to imagine that if a higher-performance CST-Greenhouse is chosen to charge the battery in the future, although the charging time may be correspondingly longer, it can power more abundant appliances to work more stably. At this point, the first step to build Greenhouse Energy scheme has been taken from the above work.

The demonstration videos of the greenhouse powering commercial devices are provided in Supplementary Video S2 and S3.

Supplementary material related to this article can be found online at [doi:10.1016/j.nanoen.2021.106328](https://doi.org/10.1016/j.nanoen.2021.106328).

Supplementary material related to this article can be found online at [doi:10.1016/j.nanoen.2021.106328](https://doi.org/10.1016/j.nanoen.2021.106328).

3. Conclusion

Aiming at the combination of intelligent agriculture and distributed energy, taking agricultural greenhouses as the research object, this work has proposed a new type greenhouse based on TENG (CST-Greenhouse). CST-Greenhouse can harvest environmental mechanical energy

including wind energy. CST-Greenhouse has an iconic arched structure that can vibrate symmetrically, constituting a contact-separation mode TENG. This fully exploits the additional function of the huge and transparent polymer films to convert environmental mechanical energy (such as wind energy) into electrical energy. CST-Greenhouse combines both charge pump and power management technology (switch circuit) to achieve an effective improvement in output. In the laboratory, only a small-scale test model was made with a simplified process to verify its feasibility, but the expected output performance and application performance have been exactly shown. Under 25 mm movement amplitude, 5 Hz vibration frequency and 100 M Ω load resistance, the maximum current is 1.31 μA , the peak output power is 107.09 μW . Thereby the unit area power is 3.06 mW/m². After charging the capacitors for about 500 s under 2 Hz, commercial devices such as temperature sensors and humidity sensors can be powered for about 20 s. This is sufficient to verify the feasibility of CST-Greenhouse supplying sensors for intermittent operation. And this work also marks the first step to build Greenhouse Energy scheme. Here, some reasonable estimates are made based on the numerical result of the above verification experiment. According to statistics, as of January 2019, the World Greenhouse Vegetable area is estimated to be 496,800 ha. (1,228,000 ac.) [55]. Therefore, it is expected that this CST-Greenhouse can provide about 15.2 MW of electricity worldwide under ideal conditions. Of course, in fact, due to the leakage effect at the edge, the output may not increase linearly with the increase of the film area [56]. Therefore, in practical applications, the greenhouse film should be arranged in reasonable segments and intervals, and the ratio of the main TENG to the pump TENG should be optimized, but these adjustment measures do not affect the overall structure of CST-Greenhouse. In addition, Greenhouse Energy combined with greenhouses is a distributed energy source, with lower transmission loss, which means it can be more directly supplied to agricultural production.

This work still has some deficiencies. For example, the motion mode of CST-Greenhouse might lead to structural fatigue, thereby affecting the service life. In addition, the material cost is not economical enough, including expensive ITO electrode film. Limited by cost, the scale of experimental CST-Greenhouse is relatively small. The output performance is not satisfactory enough, making it unable to maintain the sensor for continuous operation. All of these deficiencies need further research in the future. And overcoming the above shortcomings is also the focus of future work.

On the other hand, as above-mentioned, the experimental test-model only uses the most basic manufacturing technology. However, in future experiments or actual production, if better materials, more sophisticated technology, more meticulous material processing, more efficient circuit management and other more advanced TENG output optimization technology can be taken in, the output capacity of CST-Greenhouse will get a much greater improvement. In addition to wind energy, other forms of environmental energy, such as raindrop energy and temperature difference energy, are also expected to be harvested for CST-Greenhouse in the future. At that time, it is expected to maintain the smart operation of the entire greenhouse only relying on harvesting environmental energy. This is what truly transforms the greenhouse into a self-powered intelligent agricultural facility.

In general, the new designed CST-Greenhouse, as a verification example of the combining TENG and greenhouse, effectively utilizes the huge plastic films that have been neglected yet, and outputs considerable electrical energy. This test case converts the original "White pollution" into a power called "Greenhouse Energy", providing a new possibility for the development and design of smart greenhouses. Furthermore, the concept of Greenhouse Energy will provide guidance and inspiration for more in-depth research between TENG and agriculture, and further serve the exploration and construction of intelligent agriculture for the future life. CST-Greenhouse is exactly the first good practice of this new concept. In the end, in the exploration of combining TENG with distributed energy, in pace with Blue Energy being a

representative pioneer, Greenhouse Energy, as a new concept in agriculture, is also expected to become such a guiding and enlightening attempt. Greenhouse Energy will never be independent and non-exclusive. It is always a concept that can coexist and be inclusive with other energy concepts, including Blue Energy. In other words, Greenhouse Energy will collaborate with Blue Energy and complement the new distributed energy system starting from the agricultural field.

4. Methods and materials

4.1. Fabrication of CST-greenhouse

- 1) Greenhouse film structure. The thickness of PET and PE are 50 μm and 30 μm respectively. The transparent and flexible electrode material ITO is deposited on the PET substrate, and its thickness is negligible. Sponge is used as a buffer material to ensure that the greenhouse films are fully contacted, of which the thickness is 2 mm. The length and width of the composite film composed of the above-mentioned multilayer film are all 200 mm * 157 mm. The copper tapes are connected to the ITO surface as the external interface of the electrode with a thickness of 88 μm . A small amount of Kapton tape is used to insulate the periphery of the electrode.
- 2) Greenhouse structure. In this small-scale greenhouse model, the structure of Main TENG and Pump TENG are consistent to meet the actual needs of combining together. All frames are made by 3D printing. The printing material is ABS resin. Among them, the arched keel of the fixed frame has an outer diameter of 224 mm, an inner diameter of 216 mm and a rectangular section of 5 mm * 4 mm. The rectangular section of the mid-longitudinal-beam of the fixed frame is 10 mm * 5 mm. There are brackets for mounting bearings at both ends. The inner and outer diameters of the secondary longitudinal-beams are consistent with the keel, and the angle between the waists of the section is 2°.

In order to make the movable frame as light as possible, the arched keels of the movable frame have an outer diameter of 234 mm, an inner diameter of 230 mm and a rectangular section of 5 mm * 2 mm. In order to ensure the structural strength, the section of the secondary longitudinal-beam is approximately T-shaped, as shown in Fig. S8. In order to make the keels on the two sides of the movable frame have a certain opening angle, the cross section of movable frame's mid-longitudinal-beam is a trapezoid with an angle of 12° between the waists. There are cylindrical shafts at both ends of mid-longitudinal-beam for connecting bearings. The model is designed with standard parts in the longitudinal direction, so the number of segments can be flexibly selected according to laboratory conditions and needs, thereby changing the length of the greenhouse. In this experiment, the length of Main TENG is 200 mm, while the length of Pump TENG is 100 mm. Under gravity conditions, the movable frame will stabilize to an equilibrium position. When wind or other environmental disturbances exist, the movable frame will have periodical vibration, thereby generating alternating voltage and current.

- 3) Circuit components. Integrating on breadboard. The diode models used in the rectification and switching circuits are 1N4007. In the switching circuit, the capacitance of capacitors is 47 μF . The breakdown voltage is 50 V. The inductance used to stabilize the output is 4.7 MH.
- 4) Attachment structure. The bearing is MR106ZZ of NSK, of which the outer diameter * inner diameter * thickness is 10 mm * 6 mm * 3 mm.

4.2. Electrical output measurement

A linear motor is used to simulate the external disturbance. The model is LINMOT (version P01-37 \times 120-C/C1100, The LinMot. Inc., USA), as shown in Fig. S6. The thermal anemometer is AR866A (SMART

SENSOR). In order to ensure the consistent movement of the greenhouse frame, a baffle with a size of 350 mm * 35 mm is installed on the linear motor push head. In order to measure the electrical output of TENG, a programmable electrometer (Keithley 6514) was used.

Supplementary information

The Supplementary Information is available free of charge at (Website).

Changes in capacitance and required external force during movement; Photograph of CST-Greenhouse experimental model; The effective output of CST-Greenhouse with different load resistance and frequencies; Photograph of experimental devices; Photograph and illustration of power supply circuit; View of the secondary longitudinal-beam; Maximum amplitude with different movable frame angle; COMSOL electrical simulation for CST-Greenhouse (PDF).

CRediT authorship contribution statement

H. W. and M. Z. contribute equally to this work. J. C., H. W., L. J., and Z.L. W. conceived the idea and guided the project. H. W. and J. C. were in charge of the overall design and fabrication of CST-Greenhouse, experiments, data recording, and analysis. M. Z., Z. Y. and Z. W. contributed with ideas for the experimental designs and assisted with the measurement of mechanical and electrical characteristics. M. Z., Z. Y. and X. L. assisted with the fabrication of CST-Greenhouse and the video records of experimental results. M. Z. and Y. L. contributed to the data processing, and the description of results. All the authors discussed the results and prepared the manuscript.

Declaration of Competing Interest

The authors declare that they have no known competing financial interests or personal relationships that could have appeared to influence the work reported in this paper.

Acknowledgments

This research was supported by National Natural Science Foundation of China (No. 52075286, U1613207), National Science and Technology Major Project of China (No. 2011ZX02403), National Key Research and Development Program of China (No. 2018YFF0300606) and Tsinghua University Initiative Scientific Research Program (No. 20193080001).

Appendix A. Supporting information

Supplementary data associated with this article can be found in the online version at doi:10.1016/j.nanoen.2021.106328.

References

- [1] J. Bostock, H. Riley, *The Natural History of Pliny*, Volume IV (translation to English). Henry G. Bohn, London, 1856, 4.
- [2] S. Bhattacharjee, P. Bhattacharjee, S. Nath et al., Protected cultivation: a non-conventional way to double farmers income. *INDIAN FARMER*: 963.
- [3] M. McDaniel, *Handbook of Transition Metal Polymerization Catalysts: Hoff/Polymerization Catalysts*, 10 Review of Phillips Chromium Catalyst for Ethylene Polymerization. *Handbook of Transition Metal Polymerization Catalysts*, 2010: 291–446.
- [4] L.K. James, J.K. Laylin, *Nobel laureates in chemistry, 1901–1992*. Chemical Heritage Foundation, 1993.
- [5] C.S. Allardyce, C. Fankhauser, S.M. Zakeeruddin, M. Grätzel, P.J. Dyson, *The influence of greenhouse-integrated photovoltaics on crop production*, *Sol. Energy* 155 (2017) 517–522.
- [6] R. Meitzner, U.S. Schubert, H. Hoppe, *Agrivoltaics—the perfect fit for the future of organic photovoltaics*, *Adv. Energy Mater.* 11 (2020), 2002551.
- [7] L. Liu, C. Guan, F. Zhang et al., A novel application for concentrator photovoltaic in the field of agriculture photovoltaics. *AIP Conference Proceedings*, 2017: 080008.
- [8] J. Xue, *Photovoltaic agriculture-new opportunity for photovoltaic applications in China*, *Renew. Sustain. Energy Rev.* 73 (2017) 1–9.

- [9] J. Chikaire, F. Nnadi, R. Nwakwasi, et al., Solar energy applications for agriculture, *J. Agric. Vet. Sci.* 2 (2010) 58–62.
- [10] J.P. Campbell, E.W. Galyean, H.R. Spreckman, Transparent solar cell and method of fabrication: Google Patents, 2001.
- [11] T. Miyazaki, A. Akisawa, T. Kashiwagi, Energy savings of office buildings by the use of semi-transparent solar cells for windows, *Renew. Energy* 30 (2005) 281–304.
- [12] J.L.H. Chau, R.-T. Chen, G.-L. Hwang, P.Y. Tsai, C.C. Lin, Transparent solar cell window module, *Sol. Energy Mater. Sol. Cells* 94 (2010) 588–591.
- [13] N.G. Park, K. Kim, Transparent solar cells based on dye-sensitized nanocrystalline semiconductors, *Phys. Status Solidi (a)* 205 (2008) 1895–1904.
- [14] C.-C. Chen, L. Dou, J. Gao, W.H. Chang, G. Li, Y. Yang, High-performance semi-transparent polymer solar cells possessing tandem structures, *Energy Environ. Sci.* 6 (2013) 2714–2720.
- [15] N.F. Jones, L. Pejchar, J.M. Kiesecker, The energy footprint: how oil, natural gas, and wind energy affect land for biodiversity and the flow of ecosystem services, *BioScience* 65 (2015) 290–301.
- [16] W. Cui, Current state and future development trend of wind power at home and abroad, *Electr. Energy Manag. Technol.* (2019) 1.
- [17] H. Holttinen, P. Meibom, A. Ortho et al., Design and operation of power systems with large amounts of wind power, first results of IEA collaboration. EWEC'2006-European Wind Energy Conference & Exhibition, 2006: 1–15.
- [18] J. Abbess, Wind Energy Variability and Intermittency in the UK. Claverton-energy.com, 2009.
- [19] F.-R. Fan, Z.-Q. Tian, Z.L. Wang, Flexible triboelectric generator, *Nano Energy* 1 (2012) 328–334.
- [20] W. Ding, J. Zhou, J. Cheng, Z. Wang, H. Guo, C. Wu, S. Xu, Z. Wu, X. Xie, Z. L. Wang, TriboPump: a low-cost, hand-powered water disinfection system, *Adv. Energy Mater.* 9 (2019), 1901320.
- [21] Q. Cui, T.-H. Le, Y.-J. Lin, Y.B. Miao, I.T. Sung, W.B. Tsai, H.Y. Chan, Z.H. Lin, H. W. Sung, A self-powered battery-driven drug delivery device that can function as a micromotor and galvanically actuate localized payload release, *Nano Energy* 66 (2019), 104120.
- [22] H. Huo, F. Liu, Y. Luo, Q. Gu, Y. Liu, Z. Wang, R. Chen, L. Ji, Y. Lu, R. Yao, J. Cheng, Triboelectric nanogenerators for electro-assisted cell printing, *Nano Energy* 67 (2020), 104150.
- [23] Y.-P. Pao, C.-C. Yu, Y.-Z. Lin, S. Chatterjee, S. Saha, N. Tiwari, Y.T. Huang, C.C. Wu, D. Choi, Z.H. Lin, Carbohydrate-protein interactions studied by solid-liquid contact electrification and its use for label-free bacterial detection, *Nano Energy* 85 (2021), 106008.
- [24] K. Wang, Y. Lu, J. Cheng, X. Zhu, L. Ji, Quantitative electrostatic force measurement and characterization based on oscillation amplitude using atomic force microscopy, *ALP Adv.* 10 (2020), 015143.
- [25] Z. Wu, W. Ding, Y. Dai, K. Dong, C. Wu, L. Zhang, Z. Lin, J. Cheng, Z.L. Wang, Self-powered multifunctional motion sensor enabled by magnetic-regulated triboelectric nanogenerator, *ACS Nano* 12 (2018) 5726–5733.
- [26] W. Ding, C. Wu, Y. Zi, H. Zou, J. Wang, J. Cheng, A.C. Wang, Z.L. Wang, Self-powered wireless optical transmission of mechanical agitation signals, *Nano Energy* 47 (2018) 566–572.
- [27] C.-M. Chiu, S.-W. Chen, Y.-P. Pao, M.Z. Huang, S.W. Chan, Z.H. Lin, A smart glove with integrated triboelectric nanogenerator for self-powered gesture recognition and language expression, *Sci. Technol. Adv. Mater.* 20 (2019) 964–971.
- [28] P. Rui, W. Zhang, Y. Zhong, X. Wei, Y. Guo, S. Shi, Y. Liao, J. Cheng, P. Wang, High-performance cylindrical pendulum shaped triboelectric nanogenerators driven by water wave energy for full-automatic and self-powered wireless hydrological monitoring system, *Nano Energy* 74 (2020), 104937.
- [29] H. Yang, M. Deng, Q. Zeng, X. Zhang, J. Hu, Q. Tang, H. Yang, C. Hu, Y. Xi, Z. L. Wang, Polydirectional microvibration energy collection for self-powered multifunctional systems based on hybridized nanogenerators, *ACS Nano* 14 (2020) 3328–3336.
- [30] F. Liu, Y. Liu, Y. Lu, Z. Wang, Y. Shi, L. Ji, J. Cheng, Electrical analysis of triboelectric nanogenerator for high voltage applications exemplified by DBD microplasma, *Nano Energy* 56 (2019) 482–493.
- [31] J. Cheng, W. Ding, Y. Zi, Y. Lu, L. Ji, F. Liu, C. Wu, Z.L. Wang, Triboelectric microplasma powered by mechanical stimuli, *Nat. Commun.* 9 (2018) 1–11.
- [32] Z. Yang, Y. Yang, F. Liu, Z. Wang, Y. Li, J. Qiu, X. Xiao, Z. Li, Y. Lu, L. Ji, Z.L. Wang, J. Cheng, Power backpack for energy harvesting and reduced load impact, *ACS Nano* 15 (2021) 2611–2623.
- [33] Z. Wang, Y. Shi, F. Liu, H. Wang, X. Liu, R. Sun, Y. Lu, L. Ji, Z.L. Wang, J. Cheng, Distributed mobile ultraviolet light sources driven by ambient mechanical stimuli, *Nano Energy* 74 (2020), 104910.
- [34] J. Wang, C. Meng, Q. Gu, M.C. Tseng, S.T. Tang, H.S. Kwok, J. Cheng, Y. Zi, Normally transparent tribo-induced smart window, *ACS Nano* 14 (2020) 3630–3639.
- [35] C. Wu, H. Tetik, J. Cheng, W. Ding, H. Guo, X. Tao, N. Zhou, Y. Zi, Z. Wu, H. Wu, D. Lin, Z.L. Wang, Electrohydrodynamic jet printing driven by a triboelectric nanogenerator, *Adv. Funct. Mater.* 29 (2019), 1901102.
- [36] Y. Zi, C. Wu, W. Ding, X. Wang, Y. Dai, J. Cheng, J. Wang, Z. Wang, Z.L. Wang, Field emission of electrons powered by a triboelectric nanogenerator, *Adv. Funct. Mater.* 28 (2018), 1800610.
- [37] H. Yang, M. Deng, Q. Tang, W. He, C. Hu, Y. Xi, R. Liu, Z.L. Wang, A nonencapsulative pendulum-like paper-based hybrid nanogenerator for energy harvesting, *Adv. Energy Mater.* 9 (2019), 1901149.
- [38] Y. Ou, X. Qu, B. Shi, et al., Recent progress on nanogenerator for implantable self-powered biomedical systems, *Life Sci. Instrum.* 15 (2017) 3–14.
- [39] H. Wang, J. Cheng, Z. Wang, L. Ji, Z.L. Wang, Triboelectric nanogenerators for human-health care, *Sci. Bull.* 66 (2021) 490–511.
- [40] Z. Liu, H. Li, B. Shi, Y. Fan, Z.L. Wang, Z. Li, Wearable and implantable triboelectric nanogenerators, *Adv. Funct. Mater.* 29 (2019), 1808820.
- [41] W. Ding, A.C. Wang, C. Wu, H. Guo, Z.L. Wang, Human-machine interfacing enabled by triboelectric nanogenerators and tribotronics, *Adv. Mater. Technol.* 4 (2019), 1800487.
- [42] Y. Zi, H. Guo, Z. Wen, M.H. Yeh, C. Hu, Z.L. Wang, Harvesting low-frequency (< 5 Hz) irregular mechanical energy: a possible killer application of triboelectric nanogenerator, *ACS Nano* 10 (2016) 4797–4805.
- [43] Z.L. Wang, On Maxwell's displacement current for energy and sensors: the origin of nanogenerators, *Mater. Today* 20 (2017) 74–82.
- [44] Z.L. Wang, T. Jiang, L. Xu, Toward the blue energy dream by triboelectric nanogenerator networks, *Nano Energy* 39 (2017) 9–23.
- [45] Z.L. Wang, Catch wave power in floating nets, *Nature* 542 (2017) 159–160.
- [46] H. Zou, Y. Zhang, L. Guo, P. Wang, X. He, G. Dai, H. Zheng, C. Chen, A.C. Wang, C. Xu, Z.L. Wang, Quantifying the triboelectric series, *Nat. Commun.* 10 (2019) 1–9.
- [47] Y. Bai, L. Xu, S. Lin, J. Luo, H. Qin, K. Han, Z.L. Wang, Charge pumping strategy for rotation and sliding type triboelectric nanogenerators, *Adv. Energy Mater.* 10 (2020), 2000605.
- [48] L. Cheng, Q. Xu, Y. Zheng, X. Jia, Y. Qin, A self-improving triboelectric nanogenerator with improved charge density and increased charge accumulation speed, *Nat. Commun.* 9 (2018) 1–8.
- [49] L. Xu, T.Z. Bu, X.D. Yang, C. Zhang, Z.L. Wang, Ultrahigh charge density realized by charge pumping at ambient conditions for triboelectric nanogenerators, *Nano Energy* 49 (2018) 625–633.
- [50] W. Liu, Z. Wang, G. Wang, G. Liu, J. Chen, X. Pu, Y. Xi, X. Wang, H. Guo, C. Hu, Z. L. Wang, Integrated charge excitation triboelectric nanogenerator, *Nat. Commun.* 10 (2019) 1–9.
- [51] R. de Alwis, K.L. Williams, M.A. Schmid, C.Y. Lai, B. Patel, S.A. Smith, J.E. Crowe, W.K. Wang, E. Harris, A.M. de Silva, Enhancing the performance of triboelectric nanogenerator through prior-charge injection and its application on self-powered anticorrosion, *Nano Energy* 10 (2014) 37–43.
- [52] C. Wang, D. Han, J. Wang, Y. Yang, X. Liu, S. Huang, X. Zhang, S. Chang, K. Wu, H. Zhong, Pumping up the charge density of a triboelectric nanogenerator by charge-shuttling, *Nat. Commun.* 11 (2020) 1–9.
- [53] X. Chen, B. Yang, J. Tian, H. Hong, Y. Du, K. Li, X. Li, N. Wang, X. Yu, X. Wei, Inflammation-free and gas-permeable on-skin triboelectric nanogenerator using soluble nanofibers, *Nano Energy* 51 (2018) 260–269.
- [54] Z.L. Wang, L. Lin, J. Chen, Triboelectric Nanogenerator, Science Press, Beijing, 2017, pp. 151–155.
- [55] I. Bostan, A. Guțu, C. Guțu-Chetușca, The photovoltaic greenhouses-a challenge for Republic of Moldova. 2019 International Conference on Electromechanical and Energy Systems (SIEMEN), 2019: 1–4.
- [56] J. Shao, Y. Yang, O. Yang, et al., Designing rules and optimization of triboelectric nanogenerator arrays, *Adv. Energy Mater.* (2021), 2100065.